Transport of conservative solutes in simulated fracture networks: 1. Synthetic data generation

Donald M. Reeves,[1] David A. Benson,[2] and Mark M. Meerschaert[3]

Received 28 March 2007; revised 14 January 2008; accepted 22 January 2008; published 6 May 2008.

[1] This paper investigates whether particle ensembles in a fractured rock domain may be adequately modeled as an operator-stable plume. If this statistical model applies to transport in fractured media, then an ensemble plume in a fractured rock domain may be modeled using the novel Fokker-Planck evolution equation of the operator-stable plume. These plumes (which include the classical multi-Gaussian as a subset) are typically characterized by power law leading-edge concentration profiles and super-Fickian growth rates. To investigate the possible correspondence of ensemble plumes to operator-stable densities, we use numerical simulations of fluid flow and solute transport through large-scale (2.5 km by 2.5 km), randomly generated fracture networks. These two-dimensional networks are generated according to fracture statistics obtained from field studies that describe fracture length, transmissivity, density, and orientation. A fracture continuum approach using MODFLOW is developed for the solution of fluid flow within the fracture network and low-permeability rock matrix, while a particle-tracking code, random walk particle method for simulating transport in heterogeneous permeable media (RWHet), is used to simulate the advective motion of conservative solutes through the model domain. By deterministically mapping individual fractures onto a highly discretized finite difference grid (1 m $\times$ 1 m $\times$ 1 m here), the MODFLOW "continuum" simulations can faithfully preserve details of the generated network and can approximate fluid flow in a discrete fracture network model. An advantage of the MODFLOW approach is that matrix permeability can be made nonzero to account for any degree of matrix flow and/or transport.

Citation: Reeves, D. M., D. A. Benson, and M. M. Meerschaert (2008), Transport of conservative solutes in simulated fracture networks: 1. Synthetic data generation, *Water Resour. Res.*, *44*, W05404, doi:10.1029/2007WR006069.

1. Introduction

[2] The ability to predict large-scale transport of solutes in fractured rock is essential for evaluating the suitability of rock masses for long-term disposal of waste including high-level radioactive waste. Fractures can serve as primary pathways for fluid flow and waste migration in a low-permeability rock mass. Transport in these ground water flow systems is dependent on rock fracture properties such as density, spatial location, permeability, length and orientation.

[3] The advection-dispersion equation (ADE) relies on volume (or ensemble) averaged parameters in an attempt to describe fractured media as an equivalent continuum [*Bear*, 1972]. The equivalent continuum assumption may only be valid for fractured media at high fracture densities [*Long et al.*, 1982]. Instead of behaving like an equivalent continuum, fractured rock masses, especially those preferred for waste disposal, are sparsely fractured [*Renshaw and Pollard*, 1994; *Munier*, 2004]. Low fracture densities restrict transport to a small subset of fractures conducive to flow [*Bour and Davy*, 1997; *Renshaw*, 1999]. In contrast to the ADE, which describes solute transport using symmetric multidimensional-Gaussian (multi-Gaussian) transition densities, both field and numerical studies indicate localized transport through discrete fractures can result in asymmetric plumes and non-Gaussian breakthrough tailing [*Schwartz et al.*, 1983; *Berkowitz and Scher*, 1997, 1998; *Becker and Shapiro*, 2000; *Painter et al.*, 2002; *Kosakowski*, 2004; *Zhang and Kang*, 2004].

[4] As an alternative to equivalent continuum models, the discrete fracture network (DFN) approach was developed to address network-scale fluid flow and solute transport behavior. This approach assumes that fluid flow through a low-permeability rock mass is controlled by interconnected fractures of a network with negligible contribution from the rock matrix [e.g., *Smith and Schwartz*, 1984; *Parney*, 1999; *Dershowitz et al.*, 1991]. Consequently, DFN simulations have been used to investigate flow and transport behavior in a wide range of fracture network types [e.g., *Smith and Schwartz*, 1984; *Parney*, 1999; *de Dreuzy et al.*, 2001a, 2001b; *Park et al.*, 2001]. Since fluid flow can only occur within fractures for a DFN simulation, detailed site characterization is required for the identification and inclusion of deterministic structures into the model domain. To enhance connectivity of deterministic structures, stochastic introduc-

[1]Desert Research Institute, Reno, Nevada, USA.
[2]Department of Geology and Geological Engineering, Colorado School of Mines, Golden, Colorado, USA.
[3]Department of Statistics and Probability, Michigan State University, East Lansing, Michigan, USA.

0043-1397/08/2007WR006069$09.00

tion of background features is commonly required for DFN simulations [*National Research Council*, 1996; *Munier*, 2004]. Computational constraints associated with solving flow through a series of fractures with variable lengths and transmissivity values generally limit DFN simulations to applications where transport scales are 100 m or less, although extensions based on particle travel statistics have been developed [*Schwartz and Smith*, 1988; *Parney*, 1999; *Benke and Painter*, 2003; *Painter and Cvetkovic*, 2005].

[5] Data from natural fracture networks suggest that above a certain lower cutoff size, fracture trace lengths follow a power law distribution:

$$P(L > l) = wl^{-a}, \tag{1}$$

where the probability of a fracture of length l, is dependent on w, a constant that depends on minimum fracture length, and a power law exponent, a, that ranges between 1 and 3 for natural fracture networks [*Davy*, 1993; *Marrett*, 1996; *Renshaw*, 1996; *Odling*, 1997; *Renshaw*, 1999; *Bonnet et al.*, 2001]. Power law distributions of fracture length lead us to examine alternative transport theories based on fractals. If $a < 2$, the variance and standard deviation of the fracture length distribution diverge, and hence these fractures do not have a distinct characteristic length. The transport of particles along infinite variance pathways may result in power law probability decline similar to (1) for the largest particle jumps. Particle jumps are defined as the distance solute particles travel over a given time interval, and hence are proportional in magnitude to the velocity field. In this case, the ensemble particle plumes may not resemble a multi-Gaussian, which is the Green's function solution (i.e., statistical motion of particles from a Dirac delta function source) of the classical, second-order, multidimensional ADE. They may, instead, resemble operator-stable plumes, which are the Green's function solutions of a fractional-order ADE [*Schumer et al.*, 2003]. In addition to trace lengths, there are many other complicating factors, such as random fracture transmissivity and fracture density, that may affect the statistics of the particle jumps or velocity field.

[6] This is the first of two papers that investigate the applicability of alternative transport models on the basis of a novel Fokker-Planck evolution equation of an operator-stable density. While numerous researchers have used numerical simulations to systematically study the influence of network parameters on flow and transport behavior in fractured media [e.g., *Schwartz et al.*, 1983; *Smith and Schwartz*, 1984; *Koudina et al.*, 1998; *Sahimi*, 1994, 1995; *Mukhopadhyay and Cushman*, 1998a, 1998b; *Huseby et al.*, 2001; *Park et al.*, 2001; *Kim et al.*, 2004], our investigation into the role of fracture network properties on solute transport most closely resembles the study of *Schwartz et al.* [1983] and *Smith and Schwartz* [1984] where ensemble particle trajectories through fracture networks with orthogonal fracture sets and exponentially distributed trace lengths exhibited non-Gaussian characteristics. We expand upon the work of *Schwartz et al.* [1983] and *Smith and Schwartz* [1984] by investigating solute transport behavior in less restrictive networks with heavy-tailed distributions of trace length, variable (often nonorthogonal) fracture set orientations, and an increase in the scale of the simulations to study plume evolution across multiple scales. In this paper we provide a brief introduction of operator-stable plumes and concentrate on the generation of stochastic fracture networks based on realistic statistics obtained from field studies of natural rock fractures, the translation of discrete fractures onto a finite difference grid for the solution of fluid flow in both the fracture network and low-permeability rock matrix, and the simulation of conservative solute motion through the resultant velocity fields.

2. Characteristics of Operator-Stable Plumes

[7] Operator-stable densities provide a model of multidimensional solute transport where solute "particles" undergo power law displacements with the possibility of different scaling exponents along multiple directions [*Schumer et al.*, 2003]. Lévy's general central limit theorem [*Meerschaert and Scheffler*, 2001]

$$\vec{X}_1 + \vec{X}_2 + \cdots + \vec{X}_n \approx n^{\mathbf{E}}\vec{Y} \tag{2}$$

describes convergence of an appropriately scaled sum of a large number of independent and identically distributed (*iid*) centered, heavy-tailed random particle displacement vectors, $\vec{X}_i$, to an operator-stable random vector, $\vec{Y}$. The multi-Gaussian follows this law and will be described shortly. Eigenvalues, $1/\alpha$, of the scaling matrix $\mathbf{E}$ are used to describe rescaling, or growth rate in the case of a "plume" of particles, along the principal scaling axes (represented by eigenvectors) of the scaling matrix.

[8] According to (2), plume growth in $\mathbb{R}^m$ is described by m eigenvectors. The largest particle displacements dominate the growth of the process. For fractured media in this study, we focus on two-dimensional (2-D) particle motion where only two eigenvectors are used to appropriately scale particle displacements, $\vec{X}_i$. Orientation of these eigenvectors is unrestricted, since the scaling matrix $\mathbf{E}$ does not need to be symmetric. Thus, the shape of operator-stable plumes can range from elliptical to highly asymmetric. In the special case that the eigenvectors lie along orthogonal coordinate axes, $n^{-\mathbf{E}} = \begin{bmatrix} n^{-1/\alpha_1} & 0 \\ 0 & n^{-1/\alpha_2} \end{bmatrix}$. If the particles are conservative and do not partition to an immobile phase, then particle motion along the ith eigenvector scales according to t^{1/α_i} [*Schumer et al.*, 2003]. Particle motion, or plume growth, in noneigenvector directions scales according to a mixture of the two scaling rates. Values of α need not be equal along both eigenvectors, as plume growth may be more rapid in one direction than another.

[9] If every component of $\vec{X}_i$ has finite variance, then $\mathbf{E} = diag(1/2, 1/2)$, and (2) is equivalent to the well-known central limit theorem, where particle displacements are described by a multi-Gaussian random vector, $\vec{Y}(\vec{\mu}, \Sigma)$, where $\vec{\mu}$ is a mean shift vector and Σ is the covariance matrix. Multi-Gaussian plumes are characterized by elliptical plume geometry with orthogonal, Fickian scaling rates proportional to $t^{1/2}$ along major and minor axes of an ellipse.

[10] The application of operator-stable densities to 2-D transport in fractured media is based on a simple model:

$$\vec{X} = C_1\vec{e}_1 + C_2\vec{e}_2, \tag{3}$$

where particle displacement, $\vec{X}$, is based on marginal distributions of particle jumps, C_i, along principal plume

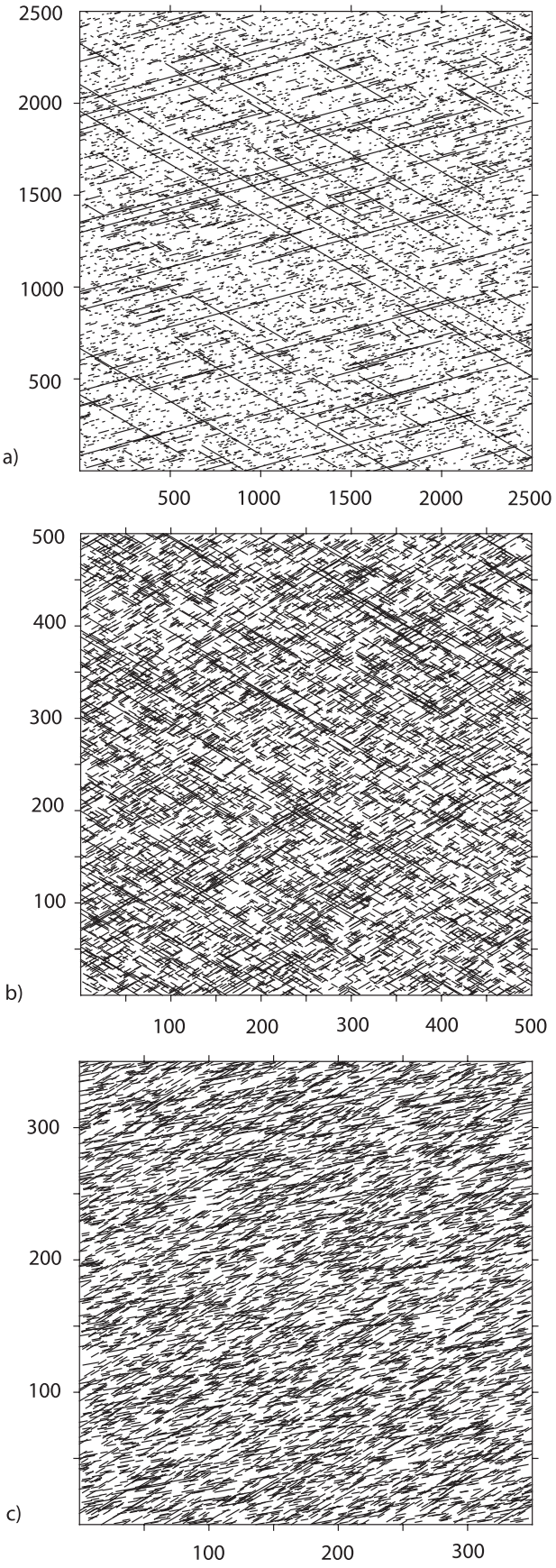

growth directions as defined by coordinate vectors (eigenvectors), $\vec{e}_i$. If the magnitudes of the particle jumps C_i are heavy tailed enough to converge to α-stable random variables, then by definition, $\vec{Y}$ is an operator-stable random vector. Conversely, if $\vec{Y}$ is multi-Gaussian, each C_i set will converge to a Gaussian [*Meerschaert and Scheffler*, 2001]. For operator-stable plumes, we conjecture that the eigenvectors may correspond to principal fracture group orientations. Multi-Gaussian plumes require orthogonal plume growth directions that may or may not correspond to nonorthogonal principal fracture group orientations [*Kim et al.*, 2004].

[11] In summary, the distinguishing properties of a non-Gaussian, 2-D, operator-stable plume are (1) the marginal distributions along the eigenvectors of the scaling matrix have power law tails, with exponents α_1 and α_2, and (2) the growth rates along the eigenvectors are super-Fickian at rates proportional to t^{1/α_1} and t^{1/α_2}. The purpose of this study is to investigate the operator-stable (including multi-Gaussian) properties of ensemble particle motions in large-scale fractured media simulations. If the plumes have operator-stable properties, then there is a possibility that ensemble transport in fractured media may be described by analytical equations of fractional order [*Schumer et al.*, 2003].

3. Simulation of Fractures, Flow, and Transport

[12] The numerical experiments consist of generating a large number of random fracture networks, solving for the velocity distributions within the fracture networks and rock matrix, and tracking particle trajectories through the model domains. Monte Carlo methodology is implemented to produce ensemble particle plumes from multiple equiprobable realizations of fluid flow and solute transport through the 2-D fracture networks.

[13] The fracture network geometry for each realization is based on realistic probability distributions for fracture placement and trace length, and an equation used to control fracture spatial densities in the model domain. The majority of fracture networks are simple and consist of two independent fracture groups with different orientations, spatial densities, and/or power law exponent for trace lengths (Figure 1). A few additional networks consider more complex scenarios where fracture group orientation is allowed to deviate around a mean orientation and/or more than two fracture groups are present.

3.1. Fracture Group Orientation

[14] These 2-D fracture network simulations are meant to approximate horizontal (map view) flow, so that each fracture is assumed to be vertical. The fracture orientations refer to the angle between the fracture and the hydraulic gradient applied at the boundaries of the model domain. Natural networks typically consist of two [e.g., *LaPointe and Hudson*, 1985; *Barton*, 1995; *Ehlen*, 2000] or several

Figure 1. Fracture network samples representing (a) sparsely fractured domains dominated by very long fractures, (b) moderately fractured domains comprising short and long fractures, and (c) densely fractured domains dominated by short fractures. For illustration purposes, the higher-density values used in Figures 1b and 1c require smaller subdomains. All values are in meters.

fracture groups [e.g., *Billaux et al.*, 1989; *Gillespie et al.*, 1993; *Odling*, 1997], with most fractures in a group oriented in nearly the same direction. To test a simple case, the majority of our fracture networks consist of two fracture groups with fixed orientations. Four simulations involve more complex networks with more than two fracture groups where the orientation of individual fractures can deviate from the dominant fracture group direction.

3.2. Fracture Trace Length

[15] Several analyses of field data from natural rock fracture networks indicate trace lengths of natural rock joints (opening/mode I) and faults (shear/mode II) are distributed according to power law models [*Davy*, 1993; *Marrett*, 1996; *Renshaw*, 1996, 1999; *Odling*, 1997; *Bonnet et al.*, 2001]. A Pareto probability distribution (1) is used in this study to assign fracture trace length. The use of a power law distribution for fracture trace length results in higher frequencies of smaller fractures with decreasing frequencies of longer fractures. To be consistent with the field studies of *Davy* [1993], *Renshaw* [1999] and *Bonnet et al.* [2001], values for the power law exponent range between 1 and 3. In general, mean fracture length and the exponent (a) are inversely related; networks with $a = 1$ are dominated by long domain-spanning fractures, while networks with $a = 3$ are dominated by very short fractures. A minimum fracture length of five times the cell length of 1 m was used in the model. This value is used in (1) for the computation of w.

3.3. Spatial Distribution of Fractures

[16] Numerical and field studies suggest that mechanical crack interaction plays a central role during fracture propagation and may control both fracture lengths and spacing in natural fracture networks [*Segall and Pollard*, 1983; *Olson*, 1993; *Ackermann and Schilsche*, 1997; *Darcel et al.*, 2003]. As a stochastic model, we chose to ignore the complexities of mechanical crack interaction as fracture lengths in natural fracture networks follow power law distributions. On the basis of field studies that suggest fracture spacing is an exponentially distributed random variable [*Rives et al.*, 1992; *Brooks et al.*, 1996; *Wines and Lilly*, 2002], a joint uniform $U(0, 2500)$ distribution is used to randomly assign the location of fracture centers within the model domain as a Poisson process [*Ross*, 1985]. This is because the spacings between *iid* uniform random variables are exponentially distributed [*Ross*, 1985].

3.4. Fracture Spatial Density

[17] Fractures are input into the model until a specified spatial density criteria is fulfilled. The spatial fracture density is computed by

$$\rho_{2D} = \frac{1}{A}\sum_{i=1}^{n} l_i, \tag{4}$$

where the density of fractures in a two-dimensional domain is computed from the sum of fracture trace lengths, l_i, and normalized by area, A. Spatial density values for the model domains are divided into three general groups: minimum, intermediate, and maximum, on the basis of the value of the power law exponent. Minimum values correspond to networks that are at, or just above, the percolation threshold and were determined from MODFLOW solutions (i.e., nonzero values for network flow and visual displays of head output). On the basis of field mapping studies in fractured rock, a spatial density value of 2.5 [*Renshaw*, 1997] and a fractal dimension of 1.8 [*Ehlen*, 2000] were used to assign maximum spatial density. Note that the maximum density value from *Renshaw* [1997] is a slightly different density metric and requires conversion to (4). Fractal dimensions of the networks were computed using a standard box counting method [*Barton*, 1995]. The use of both spatial density and fractal dimension was required because of the large range in power law exponents used to control fracture lengths. In general, the spatial density value was used as the maximum spatial density criteria for networks with lower power law exponent values, while fractal dimension was used for networks with higher power law exponents.

3.5. Fracture Transmissivity

[18] We are unaware of a study that measures both the length and transmissivity of fractures. Therefore, we assume that these quantities are uncorrelated. On the basis of results from recent hydraulic testing on boreholes at the Äspo Hard Rock Laboratory [*Gustafson and Fransson*, 2005], we use a transmissivity distribution similar to (1) with a power law exponent of $a_T = 0.4$ along with minimum and maximum values of 10^{-11} m^2/s and 10^{-2} m^2/s to randomly assign transmissivity values to individual fractures. The upper limit on transmissivity is maintained by discarding values greater than 10^{-2} m^2/s. For comparison purposes, a subset of simulations assign transmissivity values to individual fractures according to a lognormal distribution with distributional parameters estimated from the same Äspo data set.

3.6. Fracture Continuum Modeling

[19] Several researchers have used fracture continuum (FC) models to numerically simulate flow and transport in fractured media [*Neuman*, 1987; *Widén and Walker*, 1999; *Svensson*, 2001a, 2001b; *McKenna and Reeves*, 2006; *Ando et al.*, 2003; *Langevin*, 2003; *Pohlmann et al.*, 2004]. Instead of representing discrete fractures as continuous line elements in 2-D or planes in 3-D, FC models are based on the conversion of discrete fractures, or more commonly fracture zones, to permeability structures on a model grid. This conceptualization is supported by field observations that rock volumes are often intersected by a few dominant fractures [*Neuman*, 2005]. Often, the selection between a DFN and FC model is dependent on scale; DFN models are favored at smaller scales where they remain computationally feasible and FC models are used for larger-scale models. However, comparisons between DFN and FC models have shown that both methods are equally capable of capturing key aspects of flow and transport in fractured crystalline rock masses [*Svensson*, 2001b; *Selroos et al.*, 2002; *Ando et al.*, 2003].

[20] The large domain size (2.5 km by 2.5 km) used in this study is well beyond computational limits of DFN models. To assess the influence of rock fractures on plume growth, we designed a method that combines elements of both. Individual fractures are deterministically mapped onto a highly discretized finite difference grid (i.e., each cell measures 1 m $\times$ 1 m $\times$ 1 m) (Figure 2) and a four order-of-magnitude permeability contrast exists between the simulated rock matrix and the least transmissive rock fractures. The small cell size preserves details of the generated net-

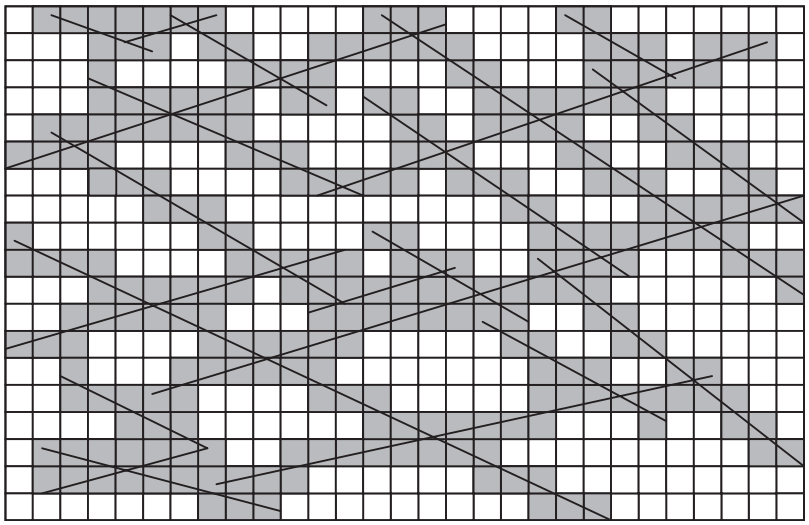

Figure 2. Finite difference representation of a hypothetical rock fracture network. Rock fractures (line segments) are overlain onto a finite difference grid. Fracture-occupied cells (gray) are assigned hydraulic properties on the basis of fracture properties, while hydraulic properties of the matrix are assigned to nonfracture-occupied cells (white). Grid discretization is for illustration purposes only.

works across all scales and the permeability contrast between the rock matrix and fractures restricts fluid flow to the fracture network. Since matrix flow is allowed, each simulation has 6.25 million active cells. MODFLOW [*McDonald and Harbaugh*, 1988] is used to solve for two-dimensional fluid flow in both the matrix and the fracture network.

[21] Though conceptually similar to a DFN simulation, mapping fractures onto a finite difference grid can enhance the connectivity of individual fractures that would otherwise not be connected in a DFN simulation. For example, two parallel unconnected fractures placed in the same finite difference cell are made connected. For our simulations, enhanced connectivity is not a concern since the cell size is much smaller than the average fracture spacing [e.g., *Svensson*, 2001b]. To further minimize the connectivity between fractures, a percolation algorithm could have been used to limit the simulations only to the individual fractures that form a hydraulic backbone. However, this would have been computationally expensive since the dense networks with short fractures can contain as many as 400,000 fractures per realization. Instead, interconnected fracture-occupied cells on a grid with a constant cell size of 1 m $\times$ 1 m $\times$ 1 m that meet a Darcy velocity criteria define the hydraulic backbone. At cells containing more than one fracture, two rules are used: (1) when fracture orientations are equal, individual fractures are parallel and fracture transmissivity values are added together to form a larger equivalent fracture, and (2) when fractures of different orientations intersect, the resultant transmissivity is based on the largest individual fracture transmissivity value. The addition of an active low-permeability matrix dramatically decreases computational demands for solving flow in the interconnected fracture network while adding only minor contributions of flow to the model domain. However, the use of a continuum grid allows us to include the effects of matrix interaction in future studies.

[22] The use of a finite difference grid to simulate discharge in a fracture that is not aligned with the grid requires an adjustment to account for longer flow paths (Figure 3). Although head values in the model domain are unaffected by the configuration of the fracture equivalents, longer flow paths due to both horizontal and vertical flow components reduce the hydraulic gradient from cell to cell along the "stair step" pattern. Transmissivity values must be increased to correct for the gradient so that proper discharge values can be obtained in each fracture. In two dimensions, the transmissivity input into MODFLOW is

$$T_{MODFLOW} = [\sin|\theta| + \cos|\theta|] \cdot T_{fracture}, \quad (5)$$

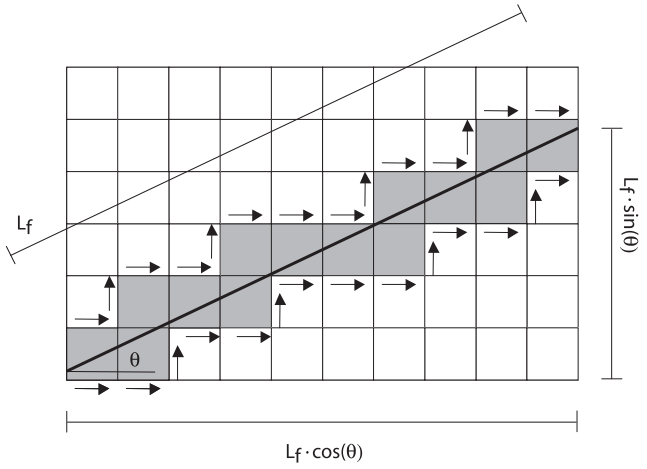

Figure 3. Flow through a fracture equivalent on a finite difference grid consisting of both horizontal and vertical flow components (denoted by arrows) resulting in a "stair step" pattern and a longer flow path than that of the original fracture, L_f. The relationship between the equivalent flow path, L_e, for a fracture of length L_f oriented θ degrees from horizontal is $L_e = L_f[\sin|\theta| + \cos|\theta|]$.

Table 1. Flux Comparison Between a Discrete Fracture and a Finite Difference Fracture Equivalent

θ,[a] deg	$q_{fracture}$[b]	$q_{MODFLOW}$[c]	Percent Error
0	1.000×10^{-10}	1.001×10^{-10}	0.01
5	9.962×10^{-11}	9.968×10^{-11}	0.06
10	9.848×10^{-11}	9.852×10^{-11}	0.05
15	9.659×10^{-11}	9.668×10^{-11}	0.09
20	9.397×10^{-11}	9.406×10^{-11}	0.10
25	9.063×10^{-11}	9.072×10^{-11}	0.10
30	8.660×10^{-11}	8.670×10^{-11}	0.12
35	8.192×10^{-11}	8.199×10^{-11}	0.09
40	7.660×10^{-11}	7.666×10^{-11}	0.07
45	7.071×10^{-11}	7.078×10^{-11}	0.10
50	6.428×10^{-11}	6.430×10^{-11}	0.04
55	5.736×10^{-11}	5.736×10^{-11}	0.01
60	5.000×10^{-11}	4.999×10^{-11}	0.02
65	4.226×10^{-11}	4.227×10^{-11}	0.02
70	3.420×10^{-11}	3.421×10^{-11}	0.03
75	2.588×10^{-11}	2.589×10^{-11}	0.04
80	1.736×10^{-11}	1.743×10^{-11}	0.04
85	8.716×10^{-12}	8.760×10^{-12}	0.05

[a]Fracture orientation from hydraulic gradient.
[b]Discharge [m/s] through a discrete fracture with $K = 1.0 \times 10^{-8}$ m/s and a hydraulic gradient of 0.01.
[c]Discharge [m/s] through a MODFLOW fracture equivalent.

where θ is fracture orientation from the horizontal gradient. Once fracture transmissivity is adjusted, the measured error between flow for a straight-line fracture and its MODFLOW equivalent is less than 0.2% (Table 1). Given a four order-of-magnitude contrast between transmissivity values for matrix and fracture cells (i.e., the smallest transmissivity contrast possible for these simulations), the flow solution accurately matches the analytical flow value for a single fracture. This indicates that the flow fields produced by the fracture continuum method in this study can be used to accurately simulate both trailing and leading edges of a contaminant plume.

[23] All model domain boundaries are constant head, inducing mean fluid flow from left to right according to a linear hydraulic gradient of 0.01. The boundary configuration represents an unbounded fractured rock mass where both fluid and solutes can exit any down gradient boundary. Because of the large-scale nature of these simulations (over 6 million cells), the Advanced Computing in the Environmental Sciences (ACES) supercomputer located at the Desert Research Institute, Reno, Nevada, was used to solve the steady state groundwater flow equation for multiple fracture network realizations.

3.7. Particle Tracking

[24] The random walk particle method for simulating transport in heterogeneous permeable media (RWHet) solves an advection-dispersion equation on a finite difference grid using a random walk particle method [*LaBolle et al.*, 1996; E. M. LaBolle, RWHet: Random walk particle model for simulating transport in heterogeneous permeable media, version 2.0 user's manual and program documentation, 2000]. The advective motion implemented by RWHet consists of the calculation of a series of independent, conservative solute particle trajectories based on bilinear interpolation of the velocity field with respect to particle location [*LaBolle et al.*, 1996].

[25] We use RWHet to track particles through the flow fields using advective transport only. The bilinear interpolation scheme introduces microdispersion due to differential velocities within single fractures, while macrodispersion is caused by the wide range of flow velocities for individual fractures and geometry of the hydraulic backbone. Within-fracture dispersion increases with transport distance and varies according to orientation. On the basis of particle-tracking tests through a single fracture, within-fracture longitudinal dispersivity at a transport scale of 100 m ranges from 10^{-8} m for fractures aligned with the hydraulic gradient to a maximum of 10^{-1} m for fractures oriented at 45° from the gradient. These values are essentially negligible and particles migrate as near piston flow "slugs" through individual fractures (Figure 4). The particle locations are recorded for 16 time steps on the basis of equal log cycle time increments for 6 log cycles. Emphasis is placed on early time steps when particles with rapid trajectories are still within the model domain. Actual log cycle times depend on distributions of trace length; particle positions are first recorded at 0.1 years for sets dominated by longer fractures and 10 years for all other sets.

[26] A unique transmissivity value is assigned to each finite difference cell containing at least one fracture. Since a rock fracture physically occupies only a small volume of a 1m by 1m by 1m cell, a porosity relationship for each fracture-occupied cell is computed on the basis of cell size and transport aperture (Figure 5). For our simulations, porosity is equivalent to transport aperture. We use *Dershowitz et al.*'s [1999] empirical quadratic law

$$b = 0.25T^{\frac{1}{2}}, \tag{6}$$

where b [m] is the transport aperture, and T [m^2/s] is the transmissivity of a fracture occupied cell, which the authors argue gives better estimates of transport aperture than the cubic law.

[27] Similar to the calculation of discharge in a finite difference setting, an adjustment is needed to correctly calculate the particle velocity. Since the particle must travel a longer path in the model than in the "real" fracture, it must be sped up by the length ratio of the hypotenuse to the sides of a right triangle. This speed is adjusted through each cell's porosity. The correction factor used in (5) overestimates a typical particle's path length since it assumes that a particle goes around corners at right angles. We correct the distance by assuming that the mean particle path is semi-circular around corners (Figure 3) with a length of $\pi/4$ times the cell length. The total correction for a fracture oriented θ degrees from horizontal mapped onto a grid with a cell size of 1 m by 1 m by 1 m (Figure 6) is

$$f = \frac{L_e}{L_f} = \frac{\pi/2 + (\tan|\theta|)^d - 1}{\sqrt{(\tan|\theta|)^{2d} + 1}}, \tag{7}$$

where $d = -1$ when $-45° \leq \theta \leq 45°$ and $d = 1$ when $45° < \theta < 90°$ or $-90° < \theta < -45°$. Using (7), effective porosity values for RWHet are then computed:

$$n_e = F \cdot b. \tag{8}$$

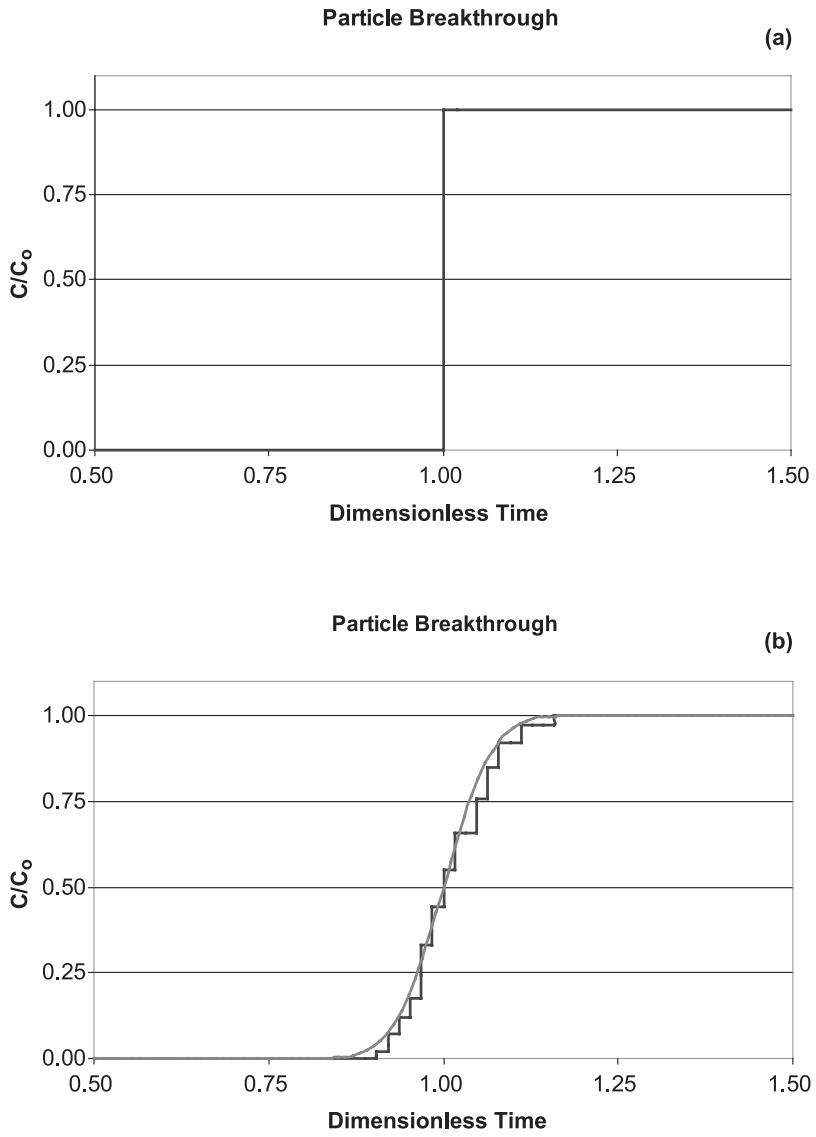

Figure 4. Normalized particle breakthrough curves for fractures with equivalent length (50 m), transmissivity (1.0×10^{-8} m^2/s), and transport aperture (2.5×10^{-5} m) oriented at (a) 0° and (b) 45° demonstrate that particles migrate as near-piston flow "slugs" through individual fractures. Note that the lighter curve in Figure 4b represents a best fit Gaussian with a mean and standard deviation of 1.0 and 5.5×10^{-2} dimensionless time units, respectively.

[28] Numerical tests on individual fractures show that errors for velocity using (8) vary according to the position of a particle relative to the cell boundaries but are less than 10%. These errors manifest themselves as the aforementioned numerical "microdispersivity" ranging from 10^{-8} to 10^{-1} m.

[29] The placement of particles in the model domain is intended to be representative of a repository scenario where the possibility of the release of contaminants over a large spatial area is possible. For each realization, 25,000 conservative particles are uniformly distributed into cells representing fractures in the model domain in the form of a 100 m by 100 m box that extends from 100 m to 200 m in the x direction and 1200 m to 1300 m in the y direction (Figure 7). Particles are only placed into "active" cells located within this zone. The hydraulic backbone, which consists of the interconnected fracture network where fluid flow occurs, was not rigorously defined in this study. Criteria for "active" cell designation consists of both occupation of a cell by a fracture and cell Darcy velocities that are at least two or three orders of magnitude greater than the average matrix value. Solute particles are evenly distributed among all active cells located within the particle release area (i.e., the amount of particles released into active cells are independent of flux).

4. Ensemble Particle Displacement Plumes

[30] A total of 23 parameter sets, defined as a set of statistics used to define fracture length, orientation, and density, were generated to investigate the transport behavior in a wide variety of network types (refer to companion paper for parameter set values). The total number of realizations per parameter set is limited to 500 because of

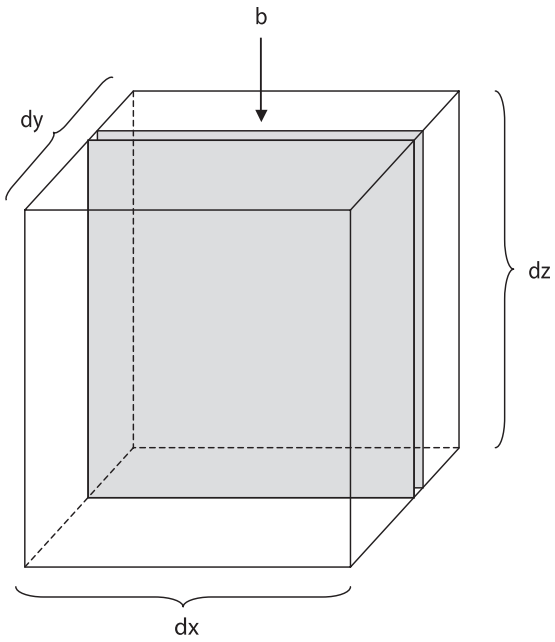

Figure 5. Porosity of fracture-occupied cell in relation to cell size and transport aperture, b. For our simulations, cell porosity = $V_{void}/V_{solid} = b$ since $dx = dy = dz = 1$.

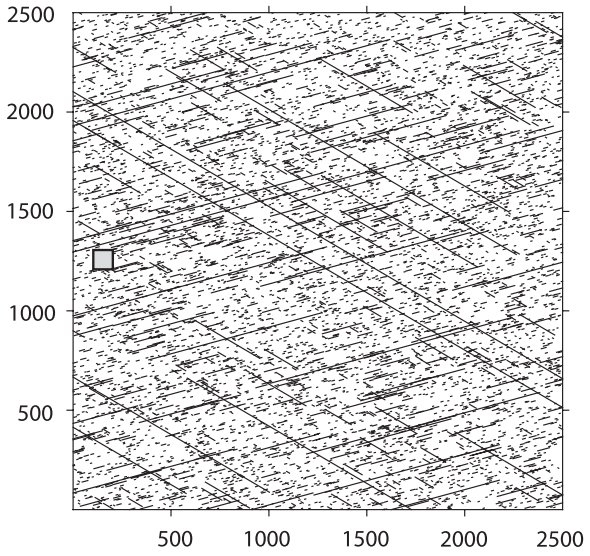

Figure 7. Fracture network domain with shaded region representing area of domain subject to introduction of solute particles. The down-gradient position of the box was selected to avoid potential boundary effects. Not all realizations have fractures of the hydraulic backbone present in the particle release area. All values are given in units of meters.

the large-scale nature of the simulations. All 500 individual realizations are used to form a single ensemble data set for the study of ensemble particle behavior and construction of ensemble concentration plumes (Figure 8).

[31] Three ensemble concentration plumes, representing each endpoint and a middle value of fracture length exponent and spatial density values, show that sparsely to moderately fractured domains engender non-Gaussian plume geometry (Figures 8a and 8b). The primary growth directions of both plumes correspond to the fracture group orientations. The combination of short fractures with high spatial density values leads to the formation of elliptical, Gaussian-like plumes (Figure 8c). The disconnected "blobs" in Figures 8a and 8b are from individual realizations and demonstrate the high degree of transport variability in sparsely to moderately fractured media. The presence of these isolated concentration contours suggests that more than 500 realizations are needed to form an ensemble concentration density with continuous contours.

[32] The process of subtracting initial particle location from final particle location deconvolves the shape of the initial particle input from a relatively large spatial area to a point source. These deconvolved particle displacements represent the Green's function of the motion process. The distributional properties of the plumes can then be analyzed by transforming the particle jumps from joint (2-D) densities to marginal densities along the eigenvectors of the plume growth. Analyses of ensemble particle displacement plumes is covered in the companion paper.

5. Conclusion

[33] Standard numerical simulators designed to model fluid flow and solute transport in porous media were used to generate synthetic data for an investigation into the influence of power law fracture trace length distributions and fracture density on ensemble plume behavior in fractured media. Fracture networks with physically realistic properties were generated according to distributions of fracture length, transmissivity, density and orientation. MODFLOW was used to solve for fluid flow in both the fracture network and rock matrix, defining an approach that combines the strengths of both continuum and DFN meth-

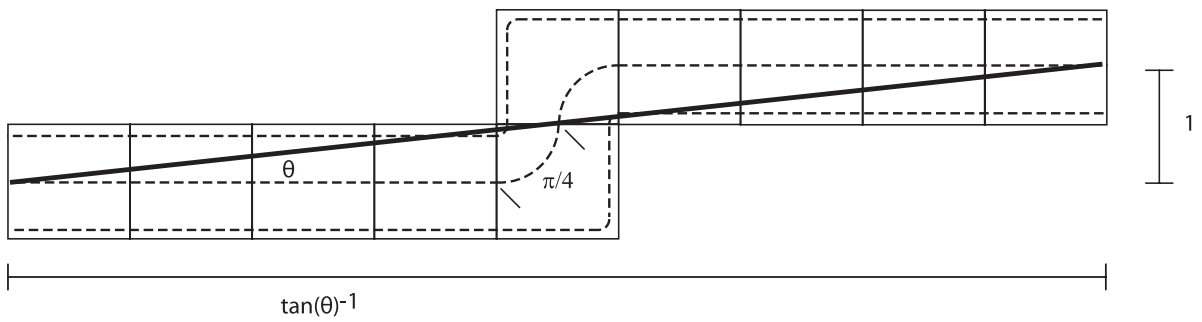

Figure 6. Idealized particle trajectories (dashed lines) in relation to straight-line distance (solid line) for a given orientation, θ. Mean curved segment length is assumed to be $\pi/4$.

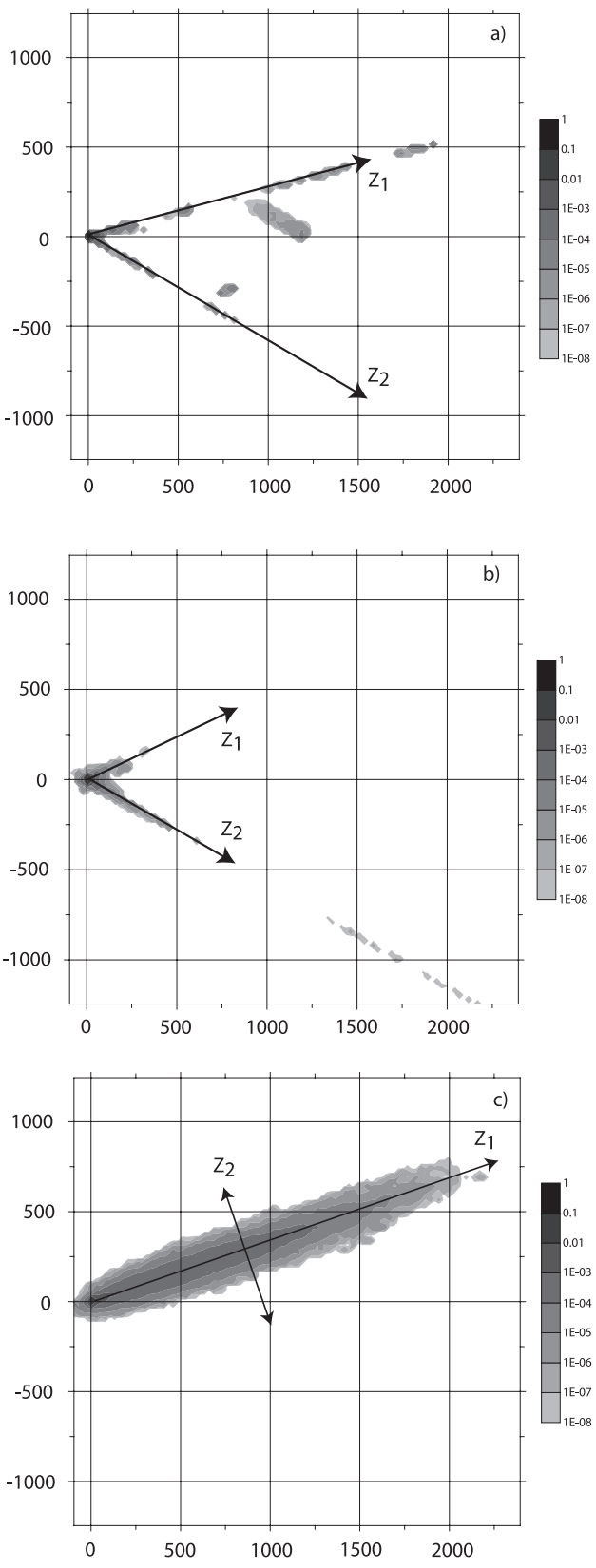

Figure 8. Ensemble displacement concentration plumes based on (a) network type in Figure 1a at a transport time of 10 years, (b) network type in Figure 1b at a transport time of 46 years, and (c) network type in Figure 1c at a transport time of 2154 years. Principal plume growth directions are denoted as Z_1 and Z_2. All spatial values are in meters.

odology. A very small cell size preserves details of fracture networks, while a permeability contrast between fractures and the matrix restricts most of the flow to fracture networks. The use of a correction factor based on fracture orientation negates error (<0.2%) between flow through a MODFLOW finite difference fracture equivalent and a discrete fracture. A random walk particle-tracking code, RWHet, was used to track advective particle trajectories through the fracture equivalents according to a bilinear velocity interpolation scheme. A correction factor based on curved streamlines was used to correct for particle velocity. After this correction, velocity error is less than 10% and is manifested as local numerical dispersion. The longitudinal dispersivity at a transport scale of 100 m ranges between 10^{-8} and 0.1 m. Ensemble particle displacement plumes, consisting of 500 possible realizations each, range from elliptical in shape with orthogonal principal axes to asymmetric "boomerang" shapes with nonorthogonal arms. Analysis of the convergence of ensemble particle jumps to either operator-stable or multi-Gaussian random vectors is the subject of a companion paper.

[34] **Acknowledgments.** This research was sponsored by grant DE-FG-02-07ER5841 from the Chemical Sciences, Geosciences, and Biosciences Division, Office of Basic Energy Sciences, Office of Science, U.S. Department of Energy; NSF grants DMS-0539176, EAR-9980489, and DMS-0139943; Desert Research Institute G. B. Maxey and NSF EPSCoR ACES fellowships; and the Marsden Fund, administered by the Royal Society of New Zealand. The DRI ACES supercomputer was essential for the numerical component of this research. We thank Eric LaBolle for making helpful modifications to his particle-tracking code and three anonymous reviewers for their helpful comments.

References

Ackermann, R. V., and R. W. Schlische (1997), Anitclustering of small normal faults around larger faults, *Geology*, *25*(12), 1127–1130.

Ando, K., A. Kostner, and S. P. Neuman (2003), Stochastic continuum modeling of flow and transport in a crystalline rock mass: Fanas-Augres, France, revisited, *Hydrogeol. J.*, *11*, 521–535.

Barton, C. C. (1995), Fractal analysis of scaling and spatial clustering of fractures, in *Fractals in the Earth Sciences*, edited by C. C. Barton and P. R. LaPointe, pp. 141–178, Plenum, New York.

Bear, J. (1972), *Dynamics of Fluids in Porous Media*, Dover, New York.

Becker, M. W., and A. M. Shapiro (2000), Tracer transport in fractured crystalline rock: Evidence of non-diffusive breakthrough tailing, *Water Resour. Res.*, *36*(7), 1677–1686.

Benke, R., and S. Painter (2003), Modeling conservative tracer transport in fracture networks with a hybrid approach based on the Boltzmann transport equation, *Water Resour. Res.*, *39*(11), 1324, doi:10.1029/2003WR001966.

Berkowitz, B., and H. Scher (1997), Anomalous transport in random fracture networks, *Phys. Rev. Lett.*, *79*(20), 4038–4041.

Berkowitz, B., and H. Scher (1998), Theory of anomalous chemical transport in random fracture networks, *Phys. Rev. E*, *57*(5), 5858–5869.

Billaux, D. M., J. P. Chiles, and C. Hestir (1989), Three-dimensional statistical modelling of a fractured rock mass—An example from the Fanay-Augères Mine, *Int. J. Rock Mech. Min. Sci. Geomech. Abstr.*, *36*(3–4), 281–299.

Bonnet, E., O. Bour, N. E. Odling, P. Davy, I. Main, P. Cowie, and B. Berkowitz (2001), Scaling of fracture systems in geologic media, *Rev. Geophys.*, *39*(3), 347–383.

Bour, O., and P. Davy (1997), Connectivity of random fault networks following a power law fault length distribution, *Water Resour. Res.*, *33*(7), 1567–1583.

Brooks, B. A., R. W. Allmendinger, and G. I. de al Barra (1996), Fault spacing in the El Teniente Mine, central Chile: Evidence of nonfractal fault geometry, *J. Geophys. Res.*, *101*(B6), 13,633–13,653.

Darcel, C., O. Bour, and P. Davy (2003), Cross correlation between length and position in real fracture networks, *Geophys. Res. Lett.*, *30*(12), 1650, doi:10.1029/2003GL017174.

Davy, P. (1993), On the frequency-length distribution of the San Andreas fault system, *J. Geophys. Res.*, *98*(B7), 12,141–12,151.

de Dreuzy, J.-R., P. Davy, and O. Bour (2001a), Hydraulic properties of two-dimensional random fracture networks follwing a power law length distribution: 1. Effective connectivity, *Water Resour. Res.*, *37*(8), 2065–2078.

de Dreuzy, J.-R., P. Davy, and O. Bour (2001b), Hydraulic properties of two-dimensional random fracture networks follwing a power law length distribution: 2. Permeability of networks based on lognormal distribution of apertures, *Water Resour. Res.*, *37*(8), 2079–2095.

Dershowitz, B., T. Eiben, S. Follin, and J. Anderson (1999), SR 97—Alternative models project, discrete fracture network modeling for performance assessment of Aberg, *Rep. R 99-43*, Swed. Nucl. Fuel and Waste Manage., Stockholm.

Dershowitz, W., P. Wallmann, and S. Kindred (1991), Discrete fracture network modeling of tracer migration experiments at the SCV site, *SKB Rep. 91-23*, Swed. Nucl. Fuel and Waste Manage., Stockholm.

Ehlen, J. (2000), Fractal analysis of joint patterns in granite, *Int. J. Rock Mech. Min. Sci.*, *37*, 909–922.

Gillespie, P. A., C. B. Howard, J. J. Walsh, and J. Watterson (1993), Measurement and characterization of spatial distributions of fractures, *Tectonophysics*, *226*, 113–141.

Gustafson, G., and A. Fransson (2005), The use of the Pareto distribution for fracture transmissivity assessment, *Hydrogeol. J.*, *14*, 15–20, doi:10.1007/s10040-005-0440-y.

Huseby, O., J.-F. Thovert, and P. M. Adler (2001), Dispersion in three-dimensional networks, *Phys. Fluids*, *13*(3), 594–615.

Kim, J., F. W. Schwartz, L. Smith, and M. Ibaraki (2004), Complex dispersion in simple fractured media, *Water Resour. Res.*, *40*, W05102, doi:10.1029/2003WR002631.

Kosakowski, G. (2004), Anomalous transport of colloids and solutes in a shear zone, *J. Contam. Hydrol.*, *72*, 23–46.

Koudina, N., R. Gonzalez Garcia, and J.-F. Thovert (1998), Permeability of three-dimensional fracture networks, *Phys. Rev. E*, *57*(4), 4466–4479.

LaBolle, E. M., G. E. Fogg, and A. F. B. Thompson (1996), Random-walk simulation of transport in heterogeneous porous media: Local mass-conservation problem and implementation methods, *Water Resour. Res.*, *32*(3), 583–593.

Langevin, C. D. (2003), Stochastic ground water flow simulation with a fracture zone continuum model, *Ground Water*, *41*(5), 587–601.

LaPointe, P. R., and J. A. Hudson (1985), Characterization and interpretation of rock mass joint patterns, *Geol. Soc. Am. Spec. Pap.*, *199*.

Long, J. C. S., J. S. Remer, C. R. Wilson, and P. A. Witherspoon (1982), Porous media equivalent for networks of discontinuous fractures, *Water Resour. Res.*, *18*(3), 645–658.

Marrett, R. (1996), Aggregate properties of fracture populations, *J. Struct. Geol.*, *18*(2–3), 169–178.

McDonald, M. G., and A. W. Harbaugh (1988), A modular three-dimensional finite-difference ground-water flow model, *U. S. Geol. Surv. Tech. Water Resour. Invest.*, *Book 6*, *Chap. 2*.

McKenna, S. A., and P. C. Reeves (2006), Fractured continuum approach to stochastic permeability modeling, in *Stochastic Modeling and Geostatistics: Principles, Methods, and Case Studies*, *AAPG Comput. Appl. Geol.*, vol. 3, 2nd ed., pp. 173–186, Am. Assoc. of Pet. Geol., Tulsa, Okla.

Meerschaert, M. M., and H. P. Scheffler (2001), *Limit Distributions for Sums of Independent Random Vectors: Heavy Tails in Theory and Practice*, John Wiley, New York.

Mukhopadhyay, M., and J. H. Cushman (1998a), Monte Carlo simulation of contaminant transport: I. Long-range correlations in fracture conductivity, *Transp. Porous Media*, *31*, 145–181.

Mukhopadhyay, M., and J. H. Cushman (1998b), Monte Carlo simulation of contaminant transport: II. Morphological disorder in fracture connectivity, *Transp. Porous Media*, *31*, 183–211.

Munier, R. (2004), Statistical analysis of fracture data adapted for modelling discrete fracture networks version 2, *Rep. R 04-66*, Swed. Nucl. Fuel and Waste Manage., Stockholm.

Neuman, S. P. (1987), Stochastic continuum representation of fracture rock permeability as an alternative to the REV and fracture network concepts, in *Rock Mechanics: Proceedings of the 28th U.S. Symposium, Tucson, Arizona*, edited by I. W. Farmer et al., pp. 533–561, A. A. Balkema, Rotterdam, Netherlands.

Neuman, S. P. (2005), Trends, prospects and challenges in quantifying flow and transport through fractured rocks, *Hydrogeol. J.*, *13*, 124–147.

NRC National Research Council (1996), *Rock Fractures and Fluid Flow: Contemporary Understanding and Applications*, Natl. Acad., Washington, D. C.

Odling, N. (1997), Scaling and connectivity of joint systems in sandstones from western Norway, *J. Struct. Geol.*, *19*, 1257–1271.

Olson, J. E. (1993), Joint pattern development: Effects of subcritical fracture growth and mechanical creack interaction, *J. Geophys. Res.*, *98*(B9), 12,225–12,265.

Painter, S., and V. Cvetkovic (2005), Upscaling discrete fracture network simulations: An alternative to continuum transport models, *Water Resour. Res.*, *41*, W02002, doi:10.1029/2004WR003682.

Painter, S., V. Cvetkovic, and J. Selroos (2002), Power-law velocity distributions in fracture networks: Numerical evidence and implications for tracer transport, *Geophys. Res. Lett.*, *29*(14), 1676, doi:10.1029/2002GL014960.

Park, Y. J., J. R. De Dreuzy, K. K. Lee, and B. Berkowitz (2001), Transport and intersection mixing in random fracture neworks with power-law length distributions, *Water Resour. Res.*, *37*(11), 2493–2501.

Parney, R. W. (1999), Statistical continuum modeling of mass transport through fractured media in two and three dimensions, Ph.D. dissertation, Univ. of B. C., Vancouver, Canada.

Pohlmann, K., G. Pohll, J. Chapman, A. E. Hassan, R. Carroll, and C. Shirley (2004), Modeling to support groundwater contaminant boundaries for the Shoal underground nuclear test, *Publ. 45184*, Desert Res. Inst., Reno, Nev.

Renshaw, C. E. (1996), Influence of subcritical fracture growth on the connectivity of fracture networks, *Water Resour. Res.*, *32*(6), 1519–1530.

Renshaw, C. E. (1997), Mechanical controls on the spatial density of opening-mode networks, *Geology*, *25*(10), 923–926.

Renshaw, C. E. (1999), Connectivity of joint networks with power law length distributions, *Water Resour. Res.*, *35*(9), 2661–2670.

Renshaw, C. E., and D. D. Pollard (1994), Numerical simulation of fracture set formation: A fracture mechanics model consistent with experimental observations, *J. Geophys. Res.*, *99*(B5), 9359–9372.

Rives, T., M. Razack, J.-P. Petit, and K. D. Rawnsley (1992), Joint spacing: Analogue and numerical simulations, *J. Struct. Geol.*, *14*, 925–937.

Ross, S. M. (1985), *Introduction to Probability Models*, 3rd ed., Academic, Orlando, Fla.

Sahimi, M. (1994), *Applications of Percolation Theory*, Taylor and Francis, London.

Sahimi, M. (1995), *Flow in Porous Media and Fractured Rock*, VCH, Weinheim, Germany.

Schumer, R., D. A. Benson, M. M. Meerschaert, and B. Baeumer (2003), Multiscaling fractional advection-dispersion equations and their solutions, *Water Resour. Res.*, *39*(1), 1022, doi:10.1029/2001WR001229.

Schwartz, F. W., and L. Smith (1988), A continuum approach for modeling mass transport in fractured media, *Water Resour. Res.*, *24*(8), 1360–1372.

Schwartz, F. W., L. Smith, and A. S. Crowe (1983), A stochastic analysis of macroscopic dispersion in fractured media, *Water Resour. Res.*, *19*(5), 1253–1265.

Segall, P., and D. D. Pollard (1983), Joint formation in granitic rock in the Sierra Nevada, *Geol. Soc. Am. Bull.*, *94*, 563–575.

Selroos, J.-O., D. D. Walker, A. Ström, B. Grylling, and S. Follin (2002), Comparison of alternative modelling approaches for groundwater flow in fractured rock, *J. Hydrol.*, *257*, 174–188.

Smith, L., and F. W. Schwartz (1984), An analysis on the influence of fracture geometry on mass transport in fractured media, *Water Resour. Res.*, *20*(9), 1241–1252.

Svensson, U. (2001a), A continuum representation of fracture networks, part I: Method and basic test cases, *J. Hydrol.*, *250*, 170–186.

Svensson, U. (2001b), A continuum representation of fracture networks, part II: Application to the Äspo Hard Rock laboratory, *J. Hydrol.*, *250*, 187–205.

Widén, H., and D. Walker (1999), SR 97—Alternative models project: Stochastic continuum modelling of Aberg, *SKB Rep. R-99-42*, Swed. Nucl. Fuel and Waste Manage., Stockholm.

Wines, D. R., and P. A. Lilly (2002), Measurement and analysis of rock mass discontinuity spacing and frequency in part of the Fimiston Open Pit operation in Kalgoorlie, West Australia: A case study, *Int. J. Rock Mech. Min. Sci.*, *39*, 589–602.

Zhang, D., and Q. Kang (2004), Pore scale simulation of solute transport in fractured porous media, *Geophys. Res. Lett.*, *31*, L12504, doi:10.1029/2004GL019886.

D. A. Benson, Department of Geology and Geological Engineering, Colorado School of Mines, 1500 Illinois Street, Golden, CO 80401, USA. (dbenson@mines.edu)

M. M. Meerschaert, Department of Statistics and Probability, Michigan State University, A413 Wells Hall, East Lansing, MI 48823, USA. (mcubed@stt.msu.edu)

D. M. Reeves, Desert Research Institute, 2215 Raggio Parkway, Reno, NV 89512, USA. (mreeves@dri.edu)